applied sciences

MDPI

Article

# The Influence of Tilt Angle on the Aerodynamic Performance of a Wind Turbine

**Qiang Wang [1], Kangping Liao [1,*] and Qingwei Ma [2]**

[1] College of Shipbuilding Engineering, Harbin Engineering University, Harbin 150001, China; wangqiang918@hrbeu.edu.cn

[2] School of Mathematics, Computer Sciences & Engineering, City, University of London, London EC1V 0HB, UK; q.ma@city.ac.uk

* Correspondence: liaokangping@hrbeu.edu.cn; Tel.: +86-451-8256-8147

Received: 16 May 2020; Accepted: 1 August 2020; Published: 4 August 2020


**Featured Application: This research has certain reference significance for improved wind turbine performance. It can also provide reference value for wind shear related study.**

**Abstract:** Aerodynamic performance of a wind turbine at different tilt angles was studied based on the commercial CFD software STAR-CCM+. Tilt angles of 0, 4, 8 and 12° were investigated based on uniform wind speed and wind shear. In CFD simulation, the rotating motion of blade was based on a sliding mesh. The thrust, power, lift and drag of the blade section airfoil at different tilt angles have been widely investigated herein. Meanwhile, the tip vortices and velocity profiles at different tilt angles were physically observed. In addition, the influence of the wind shear exponents and the expected value of turbulence intensity on the aerodynamic performance of the wind turbine is also further discussed. The results indicate that the change in tilt angle changes the angle of attack of the airfoil section of the wind turbine blade, which affects the thrust and power of the wind turbine. The aerodynamic performance of the wind turbine is better when the tilt angle is about 4°. Wind shear will cause the thrust and power of the wind turbine to decrease, and the effect of the wind shear exponents on the aerodynamic performance of the wind turbine is significantly greater than the expected effect of the turbulence intensity. The main purpose of the paper was to study the effect of tilt angle on the aerodynamic performance of a fixed wind turbine.

**Keywords:** wind turbine; tilt angle; unsteady aerodynamics; computational fluid dynamics

## 1. Introduction

The use of wind energy has increased over the past few decades. Today, wind energy is the fastest growing renewable energy source in the world [1]. Despite the amazing growth in the installed capacity of wind turbines in recent years, engineering and science challenges still exist [2]. The main goals in wind turbine optimization are to improve wind turbine performance and to make them more competitive on the market. Studies have shown that the wind turbine tilt angle affects the shear force and bending moment at the tower top and the blade root [3], and the interaction between the blade and the tower also affects the aerodynamic performance of the wind turbine [4]. Therefore, it is necessary to study the effect of tilt angle on wind turbine performance and analyze the characteristics of blade–tower interaction, aiming to improve the wind turbine performance.

In recent years, more and more scholars have been paying attention to the interaction between the blades and towers of wind turbines. Kim et al. [4] studied the interaction between the blade and the tower using the nonlinear vortex correction method. They concluded that as the yaw angle and wind shear exponent increase, the interaction between the blade and the tower decreases. The

influence of the tower diameter on the interaction between the blades and the tower is higher than that of the tower clearance. Meanwhile, this interaction may increase the total fatigue load at low wind speed. Guo et al. [5] used blade element moment (BEM) theory to study the interaction between the blade and tower. Their results show that the blade–tower interaction is much more significant than that of the wind shear. Wang et al. [6] researched the blade–tower interaction using computational fluid dynamics (CFD). Their research shows that the influence of the tower on the total aerodynamic performance of the upwind wind turbine is small, but the rotating blade will cause an obvious periodic drop in the front pressure of the tower. At the same time, we can see the strong interaction of blade tip vortices. Narayana et al. [7] researched the gyroscopic effect of small-scale wind turbines. Their findings show that changing the tilt angle can improve the aerodynamic performance of small-scale wind turbines. Recently, Zhao et al. [3] proposed a new wind turbine control method. In their control method, tilt angle increases as wind speed increases, with the purpose of reducing the blade loading and maintaining the power of the wind turbine at high wind speeds. Their research shows that the new control method can reduce the shear force at the top and bottom of the tower when compared with the yaw control strategy.

Many researchers have studied the effect of tilt angle on the structural performance of a wind turbine. For example, Zhao et al. [8] studied the structural performance of a two-blade downwind wind turbine at different tilt angles. However, there is little research on the effect of tilt angle on the aerodynamic performance of wind turbines. In this paper, aerodynamic performance of a wind turbine at different tilt angles is studied. All simulations are performed in CFD software STAR-CCM+ 12.02. Through a comparison of aerodynamic performance of the wind turbine at different tilt angles, the effects of tilt angle on the thrust, power and wake of the wind turbine are studied.

## 2. Numerical Modeling

### 2.1. Physical Model

In this study, the governing equation uses the unsteady Reynolds-averaged Navier–Stokes equation. The *SST* $k-\omega$ turbulence model was used in current simulations. A separated flow model was used to solve the flow equation. SIMPLE solution algorithm was used for pressure correction. Convection terms used the second-order upwind scheme. In the unsteady simulation, the time discretization used the second-order central difference scheme. In addition, due to the sliding mesh approach, no hole cutting was necessary, making the calculations more efficient than with the use of an overset mesh. Thus the sliding mesh technique was used to handle rotating motion of a blade [9].

### 2.2. Turbulence Model

The *SST* $k-\omega$ turbulence model can consider the complex flow of the adverse pressure gradient near the wall region and the flow in the free shear region. Thus, the *SST* $k-\omega$ turbulence model is suitable for simulating the rotational motion of the blade [10]. In addition, this turbulence model can accurately capture wind turbine wake [11,12].

In the Reynolds-averaged N-S equations, $\tau_{ij} = -\rho\overline{u_i' u_j'}$ refers to the Reynolds stress tensor. Reynolds stress tensor and mean strain rate tensor ($S_{ij}$) are related by the Boussinesq eddy viscosity assumption:

$$\tau_{ij} = 2\nu_t S_{ij} - \frac{2}{3}\rho k\delta_{ij} \quad (1)$$

where $\nu_t$ refers to the eddy viscosity, $\rho$ refers to the density, $k$ refers to the turbulence kinetic energy and $\delta_{ij}$ refers to the Kronecker delta function.

To provide closure equations, in the *SST* $k-\omega$ turbulence model, the turbulent kinetic energy ($k$) and specific dissipation of turbulent kinetic energy ($\omega$) also need governing transport equations, which are given as follows:

$$\frac{D\rho k}{Dt} = \tau_{ij}\frac{\partial u_i}{\partial x_j} - \beta^*\rho\omega k + \frac{\partial}{\partial x_j}\left[(\mu + \sigma_k\mu_t)\frac{\partial k}{\partial x_j}\right] \quad (2)$$

$$\frac{D\rho\omega}{Dt} = \frac{\gamma}{\nu_t}\tau_{ij}\frac{\partial u_i}{\partial x_j} - \beta\rho\omega^2 + \frac{\partial}{\partial x_j}\left[(\mu + \sigma_\omega\mu_t)\frac{\partial \omega}{\partial x_j}\right] + 2(1-F_1)\rho\sigma_{\omega 2}\frac{1}{\omega}\frac{\partial k}{\partial x_i}\frac{\partial \omega}{\partial x_j} \quad (3)$$

In the formulas above, the model coefficients are defined as follows:

$$\beta^* = F_1\beta_1{}^* + (1-F_1)\beta_2{}^* \quad (4)$$

$$\beta = F_1\beta_1 + (1-F_1)\beta_2 \quad (5)$$

$$\gamma = F_1\gamma_1 + (1-F_1)\gamma_2 \quad (6)$$

$$\sigma_k = F_1\sigma_{k1} + (1-F_1)\sigma_{k2} \quad (7)$$

$$\sigma_\omega = F_1\sigma_{\omega 1} + (1-F_1)\sigma_{\omega 2} \quad (8)$$

The blending function $F_1$ is defined as follows:

$$F_1 = \tanh\left\{\left\{\min\left[\max\left(\frac{\sqrt{k}}{\beta^*\omega y}, \frac{500\upsilon_\infty}{y^2\omega}\right), \frac{4\rho\sigma_{\omega 2}k}{CD_{k\omega}y^2}\right]\right\}^4\right\} \quad (9)$$

where $CD_{k\omega}$ refers to the cross-diffusion term, y refers to the distance to the nearest wall and $\upsilon$ refers to the kinematic viscosity. $F_1$ is equal to zero in the region away from the wall ($k-\varepsilon$ turbulence model) and one in the region near the wall ($k-\omega$ turbulence model).

The eddy viscosity is

$$\nu_t = \frac{a_1 k}{\max(a_1\omega, \Omega F_2)} \quad (10)$$

where $\Omega$ is the absolute value of the vorticity and $F_2$ is the second blending function, defined as

$$F_2 = \tanh\left[\max\left(\frac{2\sqrt{k}}{\beta^*\omega y}, \frac{500\upsilon}{y^2\omega}\right)^2\right] \quad (11)$$

A more detailed description of the *SST* $k-\omega$ turbulence model is provided in [10]. In this study, the parameters for the *SST* $k-\omega$ turbulence model are as follows:

$\sigma_{k1} = 0.85$ $\sigma_{\omega 1} = 0.5$ $\beta_1 = 0.075$ $a_1 = 0.31$ $\beta^* = 0.09$ $k = 0.41$ $\sigma_{k2} = 1$
$\sigma_{\omega 2} = 0.856$ $\beta_2 = 0.0828$ $\gamma_1 = \frac{\beta_1}{\beta^*} - \frac{\sigma_{\omega 1}k^2}{\sqrt{\beta^*}}$ $\gamma_2 = \frac{\beta_2}{\beta^*} - \frac{\sigma_{\omega 2}k^2}{\sqrt{\beta^*}}$

### 2.3. Computational Domain

The computational domain was divided into the rotating and outer domains, as shown in Figure 1. The size of the entire outer domain was 12D(x) × 5D(y) × 4D(z). The distance from the wind turbine to the velocity inlet was 3D, and the distance to the pressure outlet was 9D, where D is the diameter of the wind turbine. Due to the complex geometry of the blades, we used the trimmed cell mesh technology to generate high-quality meshes. In order to capture the complex flow around the blade, a fine mesh was used around the blade. A 10-layer boundary layer mesh was generated near the blade and the hub. The total thickness of the boundary layer was 0.03 m, and the growth rate was 1.2. A six-layer boundary layer mesh was generated near the tower and the nacelle. The total thickness of the boundary layer was 0.1 m, and the growth rate was 1.2. Figure 2b shows the refined sliding mesh regions around the blade. Figure 2c,d shows a close-up view of the blades and nacelle tower.

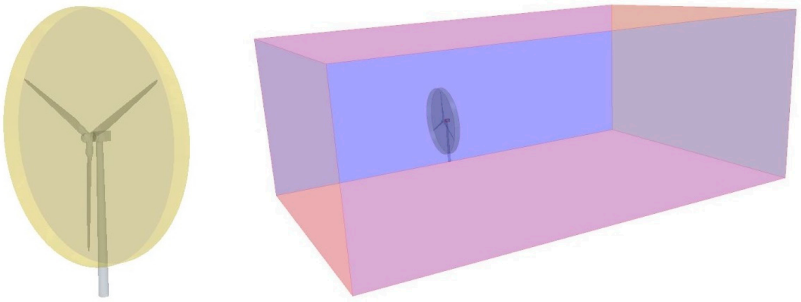

(**a**) (**b**)

**Figure 1.** Rotating and outer domain: (**a**) rotation domain for wind turbine simulation; (**b**) entire computational domain for numerical simulation.

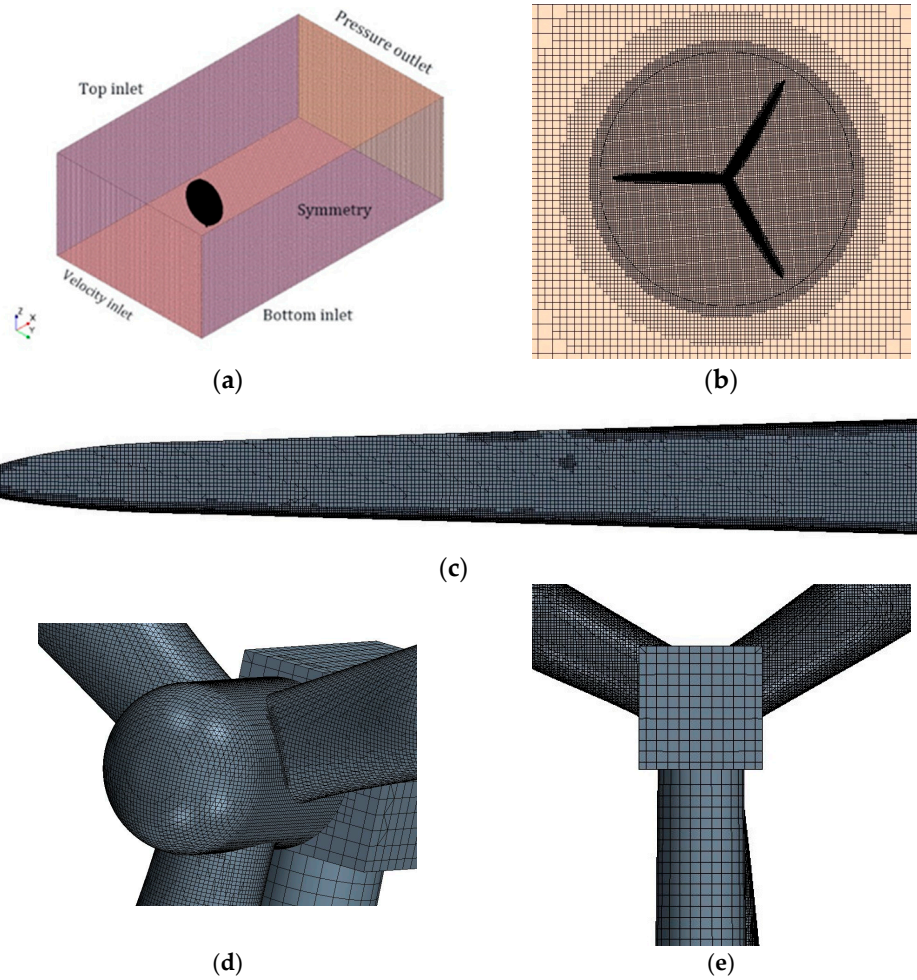


(**a**) (**b**)

(**c**)

(**d**) (**e**)

**Figure 2.** The computational mesh domain for the wind turbine: (**a**) full grid domain, (**b**) sliding mesh regions, (**c**) close-up view of the blade surface, (**d**) close-up view of the hub surface mesh and (**e**) close-up view of nacelle and tower.

### *2.4. Boundary Conditions*

Figure 2a illustrates the setting of the boundary conditions in this study. In the computational domain, the inlet boundary, bottom and top surfaces were set as velocity inlets. The pressure outlet was set at the outlet boundary. The sides of the computational domain were set to the plane of symmetry. In this simulation, all of the y+ wall treatment of near-wall modeling was applied. In order to reduce

the convergence order and improve the solution accuracy, the maximum internal iterations within each time-step was 10 [13].

## 3. Results and Discussion

### *3.1. Validations*

The 1/75 scale model of a DTU 10 MW reference wind turbine was used for the mesh independence test. In the numerical verification, the tilt angle of the wind turbine was not considered. The main parameters of the scale model are given in Table 1. A detailed introduction of the blade parameters at 40 different blade sections is provided by [14]. Figure 3 shows the wind turbine geometric model and the surface grid. After scaling according to the scale factor, the boundary layers near the blade and hub surface have five layers of refined grid with the total layer thickness of 0.004 m and a progression factor of 1.2.

**Table 1.** Principal dimensions of the scale model.

| Specifications | DTU Down-Scaled |
|---|---|
| Number of Blades | 3 |
| Rotor Diameter (m) | 2.37 |
| Hub Diameter (m) | 0.178 |
| Rated Wind Speed (m/s) | 5.53 |
| Rated Rotor Speed (rpm) | 330 |

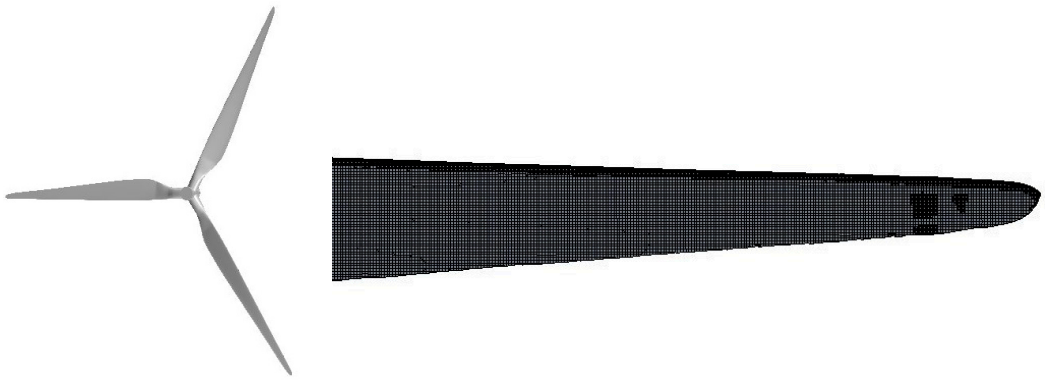

**(a)** **(b)**

**Figure 3.** Geometric model and surface grid: (**a**) the rotor geometric model; (**b**) the blade surface grid.

The blade surface mesh size includes the maximum mesh size and the minimum mesh size. The number of meshes corresponding to different mesh sizes is shown in Table 2. According to previous study, the time-step size corresponding to 1° increment of azimuth angle of the wind turbine per time-step was applied in all simulations [15]. Moreover, the simulation was run under unsteady conditions. The comparison of thrust and torque for different grid resolutions with the same wind speed of 5.53 m/s, rotor speed of 330 rpm and time-step size of $5 \times 10^{-4}$ s is presented in Tables 3 and 4. It can be observed from Tables 3 and 4 that the grid resolution of Case 3 is sufficient to solve the unsteady aerodynamics of the wind turbine. Therefore, the grid resolution of Case 3 was used in subsequent simulations.

**Table 2.** Mesh size of blade surface.

| CFD Mesh Type | Case 1 | Case 2 | Case 3 | Case 4 |
|---|---|---|---|---|
| Maximum Size (mm) | 3.000 | 2.000 | 1.500 | 1.100 |
| Minimum Size (mm) | 0.500 | 0.350 | 0.250 | 0.180 |
| Total Mesh Number (million) | 1.850 | 3.240 | 4.630 | 9.400 |

**Table 3.** Comparison of thrust between experiment and CFD simulation at different grid densities.

| CFD Mesh Type | LIFES50+ Wind Tunnel Data (N), [14] | Present Study (N) | Error (%) |
|---|---|---|---|
| Case 1 | 68.631 | 70.010 | 2.000 |
| Case 2 | | 69.660 | 1.500 |
| Case 3 | | 69.520 | 1.300 |
| Case 4 | | 69.500 | 1.300 |

**Table 4.** Comparison of torque between experiment and CFD simulation at different grid densities.

| CFD Mesh Type | LIFES50+Wind Tunnel Data (*N·M*), [14] | Present Study (*N·M*) | Error (%) |
|---|---|---|---|
| Case 1 | 6.232 | 5.690 | 8.700 |
| Case 2 | | 5.850 | 6.100 |
| Case 3 | | 5.900 | 5.300 |
| Case 4 | | 5.920 | 5.000 |

Simulations at different wind speeds were performed, and the simulation results were compared with wind tunnel experiment data, as presented in Figure 4. In this paper, we always keep the pitch angle at 0°, so we have not considered the working conditions above the rated wind speed. When the wind speed is close to the rated wind speed, the thrust and torque of the CFD simulation are lower than those of the wind tunnel experiment, but the maximum error is not more than 10%. This means that STAR-CCM+ can accurately simulate the aerodynamic performance of the wind turbine under rotating motion.

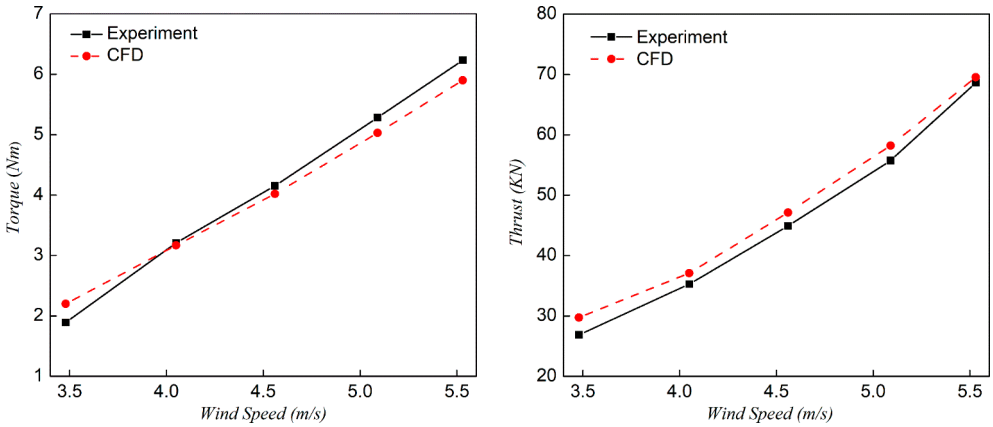


**Figure 4.** Comparison of thrust and torque between wind tunnel experiment and CFD simulation at different wind speeds (Case 3).

In order to ensure the reliability of the NREL 5 MW real-scale wind turbine simulation, the NREL 5 MW real-scale wind turbine was used for grid convergence analysis. Major properties of the NREL 5 MW reference wind turbine are given in Table 5 [16]. Figure 5 shows the blade alone geometric model and full configuration geometric model with the tower. The blade alone model was used for numerical verification, and the full configuration model was used to investigate the effect of tilt angle on the aerodynamic performance of the wind turbine. Near the wall surface of the blades and hub, the boundary layers have 10 layers of refined grid with the total layer thickness of 0.03 m and a

progression factor of 1.2. The same wind speed of 11.4 m/s and rotor speed of 12.1 rpm were applied in all simulations. Meanwhile, in all simulations, the time step is the time taken by the wind turbine to increase the azimuth angle by 1°.

**Table 5.** Principal dimensions of the NREL 5 MW reference wind turbine.

| Specifications | |
|---|---|
| Rated Power (MW) | 5 |
| Rotor Orientation, Configuration | Upwind, 3 blades |
| Rated Wind Speed (m/s) | 11.4 |
| Rated Rotor Speed (rpm) | 12.1 |
| Rotor Diameter (m) | 126 |
| Hub Diameter (m) | 3 |
| Hub Height (m) | 90 |
| Tower Base Diameter (m) | 6 |
| Tower Top Diameter (m) | 3.87 |
| Pre-cone (°) | 2.5 |

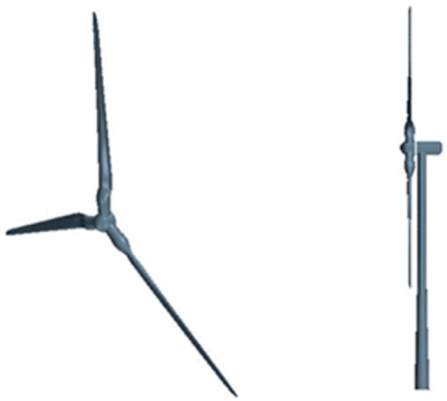

(**a**) (**b**)

**Figure 5.** Geometric model of a 5 MW reference wind turbine: (**a**) the rotor geometric model; (**b**) the full configuration model.

The number of meshes corresponding to different mesh sizes is shown in Table 6. The comparison of power for different grid resolutions with the same wind speed of 11.4 m/s and rotor speed of 12.1 rpm is presented in Table 7. It can be observed from Table 7 that the grid resolution of Case 2 is sufficient to solve the unsteady aerodynamics of the wind turbine. Therefore, the grid of Case 2 was used for the simulation of NREL 5 MW real-scale wind turbines at different wind speeds.

**Table 6.** Mesh size of blade surface.

| CFD Mesh Type | Case 1 | Case 2 | Case 3 |
|---|---|---|---|
| Maximum Size (m) | 0.20 | 0.10 | 0.05 |
| Minimum Size (m) | 0.04 | 0.02 | 0.01 |
| Total Mesh Number (Million) | 1.52 | 4.80 | 9.53 |

**Table 7.** Comparison of power between NREL data and CFD simulation at different grid densities.

| CFD Mesh Type | NREL Data (MW), [16] | Present Study (N) | Error (%) |
|---|---|---|---|
| Case 1 | 5.000 | 4.767 | 4.700 |
| Case 2 | | 4.981 | 0.380 |
| Case 3 | | 5.020 | 0.400 |

Aerodynamic simulations of a wind turbine with various wind speeds were tested and compared with the FAST results. The obtained thrust and power were compared with the corresponding NREL data calculated by FAST V8, as presented in Figure 6. The power agrees well with the NREL data, but the thrust tends to be smaller than that from NREL data. The reason for the difference between the CFD method and the FAST can be summarized as follows: (a) the FAST does not consider the three-dimensional flow effects around blades; (b) in the BEM method, in order to calculate a rotor with a limited number of blades, a tip loss correction model needs to be added. The results obtained by different tip loss correction models are also quite different [17]. FAST uses a Prandtl tip loss correction model [16]. Therefore, the CFD result of the thrust is significantly lower than the FAST result. A similar phenomenon appeared in [18]. However, at the rated wind speed, compared with FAST data, the errors of the thrust and power obtained by CFD are less than 5% Through the above analysis, the grid of Case 2 can accurately simulate the aerodynamic performance of NREL 5 MW real-scale wind turbines. Therefore, the grid of Case 2 was used to simulate the effect of tilt angle on the aerodynamic performance of the wind turbine.

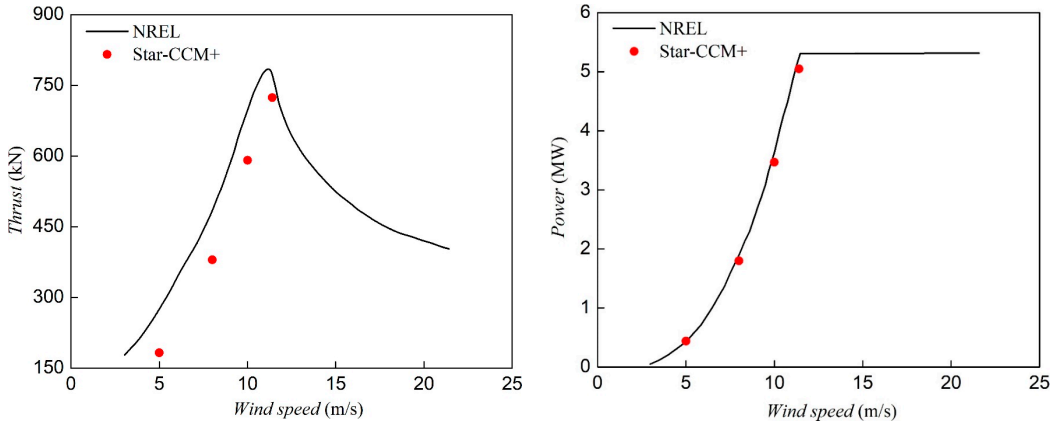


**Figure 6.** Comparisons of thrust and power.

### 3.2. The Effect of the Tilt Angle on the Aerodynamic Performance of the Wind Turbine

In this study, nacelle tilt angles of 0, 4, 8 and 12° were investigated. Figure 7 shows the structure of the wind turbine at different tilt angles. In the picture, $\beta$ is the pre-coning angle, and $\gamma$ is the shaft tilt angle. The azimuth of the rotor is defined as ψ, as presented in Figure 8. In Figure 8, the blue rotor is the initial position with the 0-azimuth angle. Subsequent analysis is based on the results after the wind turbine has stabilized. Under different tilt angles, the change in wind turbine thrust and power with the azimuth is shown in Figure 9. Comparing the no-tower curve with the other four curves, it can be seen that the thrust and power generate periodic fluctuations due to the influence of the tower. When the blades pass through the tower, the thrust and power will periodically decrease. This phenomenon is called the blade–tower interaction (BTI) [19]. The BTI effects begin at approximately 30° rotor azimuth and dissipate at approximately 100° rotor azimuth, as presented in Figure 10. This agrees with previous studies, which all show effects in approximately this same 70° range [19].

Figure 9 shows the difference between the thrust and power at approximately 60, 180 and 300° azimuth with the same nacelle tilt. This phenomenon is due to the interaction between the blade and the tower creating a random vortex. As the nacelle tilt increases, the blade and tower interactions gradually weaken. Therefore, this phenomenon becomes less important as the nacelle tilt increases. In Figure 10, when ψ is approximately 65°, the thrust and power of the wind turbine at 4 and 8° nacelle tilt are higher than 0 and 12° nacelle tilt.

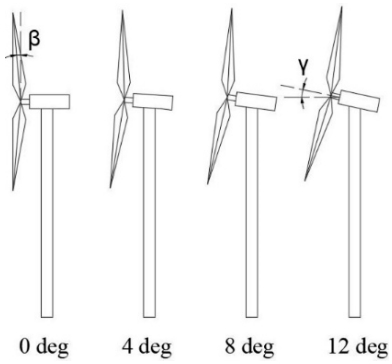


**Figure 7.** Structure of the wind turbine at different tilt angles.

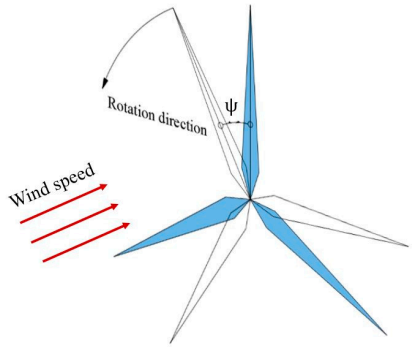


**Figure 8.** Definition of the azimuth.

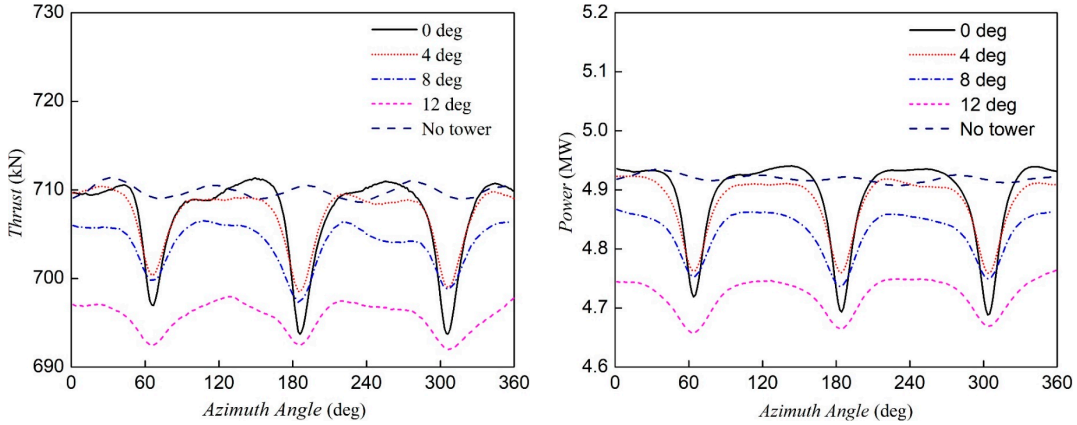


**Figure 9.** Comparison of thrust and power at different nacelle tilt angles.

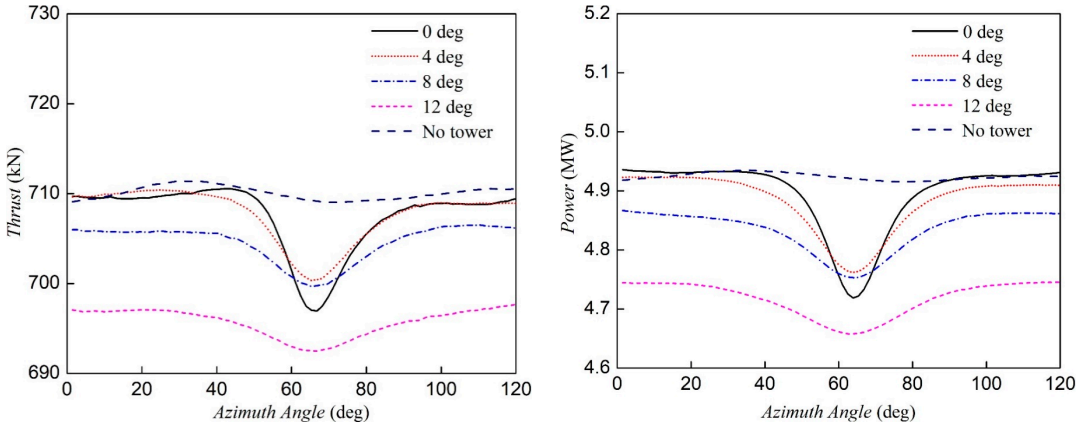


**Figure 10.** Comparison of thrust and power at different nacelle tilt angles (partial enlargement).

The position of the blade relative to the tower with the 60° azimuth is shown in Figure 11. Instantaneous pressure magnitude and streamlines at blade sections r/R = 0.5, r/R = 0.7 and r/R = 0.9 (Blade 1) of the wind turbine are presented in Figures 12–14. In the low span (r/R = 0.5) suction side, the flow separation phenomenon can be observed. However, the flow remains attached for higher radial sections (r/R = 0.7 and r/R = 0.9). In addition, with the increase of the nacelle tilt, the flow separation of the low span suction side is gradually weakened. The variation of the pressure distribution around different sections airfoil with the nacelle tilt can also be observed.

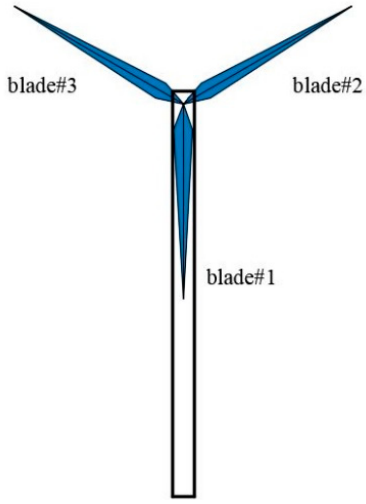


**Figure 11.** Blade position (ψ = 60°).

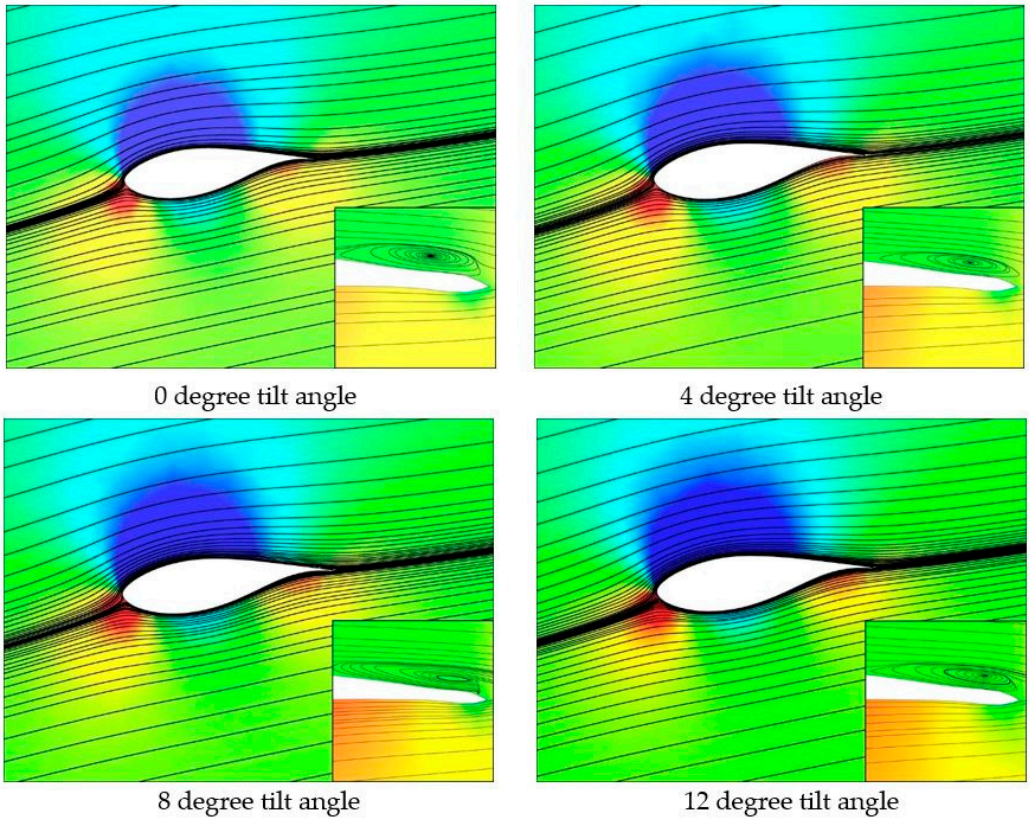


**Figure 12.** Instantaneous pressure magnitude and streamlines diagram (r/R = 0.5).

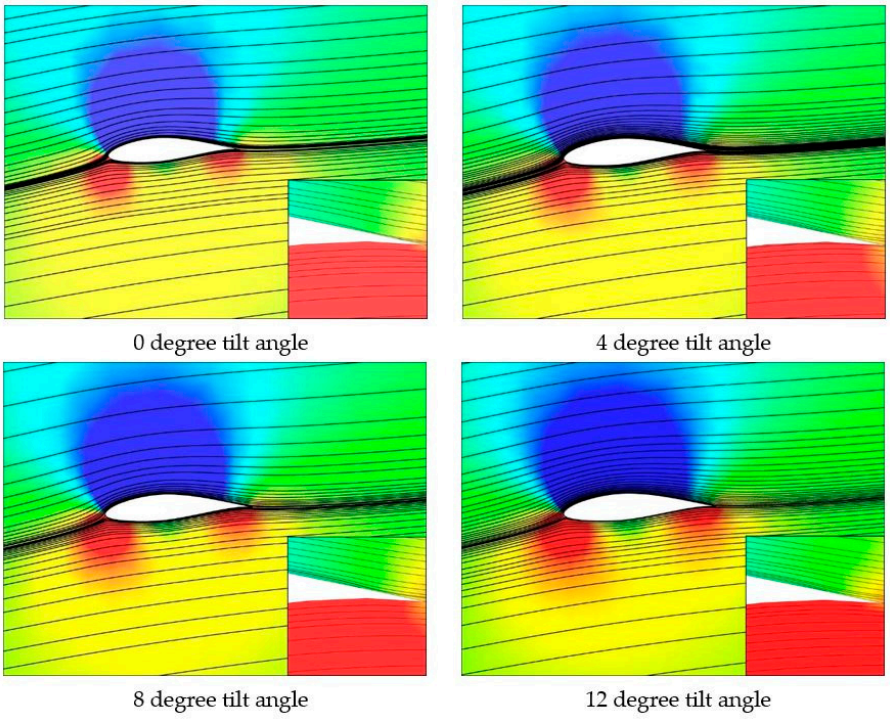


**Figure 13.** Instantaneous pressure magnitude and streamlines diagram (r/R = 0.7).

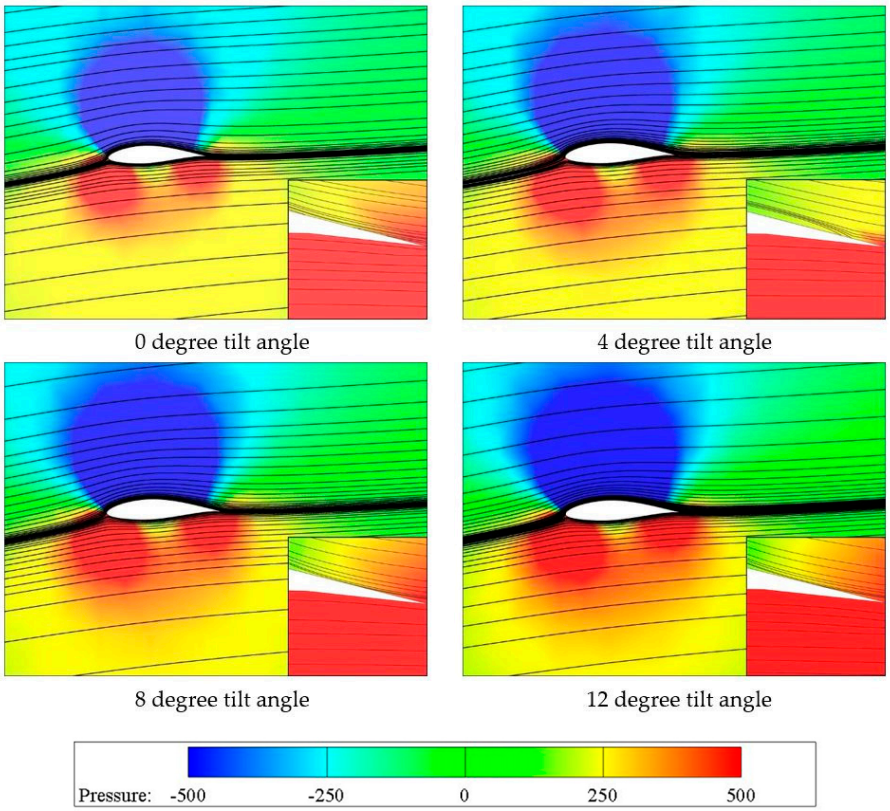


**Figure 14.** Instantaneous pressure magnitude and streamlines diagram (r/R = 0.9).

H. Rahimi et al. [20] studied different methods of calculating the angle of attack of the wind turbine section airfoil. However, in CFD, when considering the interaction between the blade and the tower, it is difficult to calculate the angle of attack of the blade section airfoil. Therefore, only the effect of tilt angle on the blade section airfoil load is considered in this paper. Figure 15 shows the

distribution of azimuth average thrust and tangential force along the blade span. From the figure, we can see that in terms of thrust, when the tilt angle is 4°, the distribution of the thrust along the blade span does not change much compared to the 0° tilt angle. However, when the tilt angle is increased to 8 and 12°, the thrust of the section airfoil at the blade tip is lower than the values at 0 and 4° tilt angle. In terms of tangential force, the tangential force gradually decreases as the tilt angle increases, for up to 0.5 of the span. However, the tangential force at 4° tilt angle does not change much compared to 0° tilt angle. Figure 16 shows the distribution of thrust and tangential force along the blade span when the blade is located in front of the tower. In terms of thrust, the thrust of the section airfoil gradually increases as the tilt angle increases, for up to 0.7 of the span. Regarding the tangential force, the increase of the tilt angle also increases the tangential force, for up to 0.6 of the span. However, regardless of thrust or tangential force, the value at 8° of tilt does not change much compared to 12° of tilt. This means that the influence of the tower becomes weaker after the tilt angle exceeds 8°.

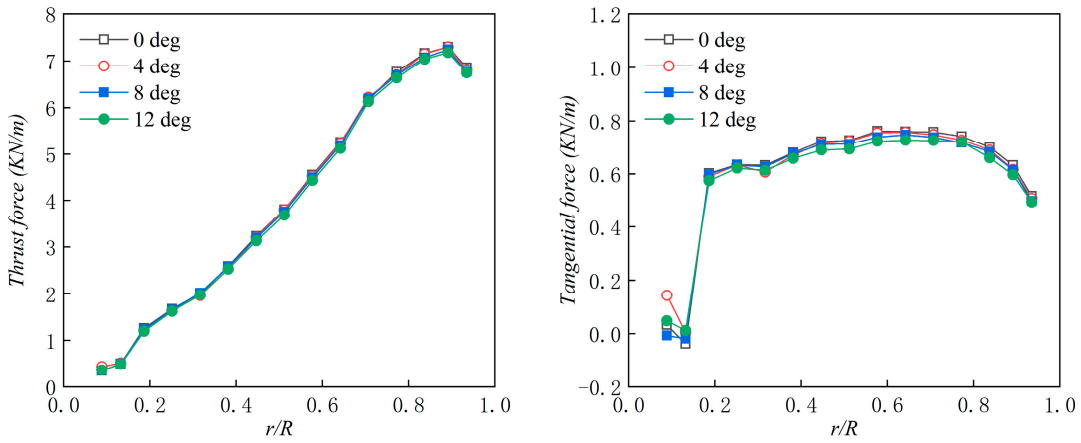


**Figure 15.** The average thrust and average tangential force per unit of span along the blade span for Blade 1.

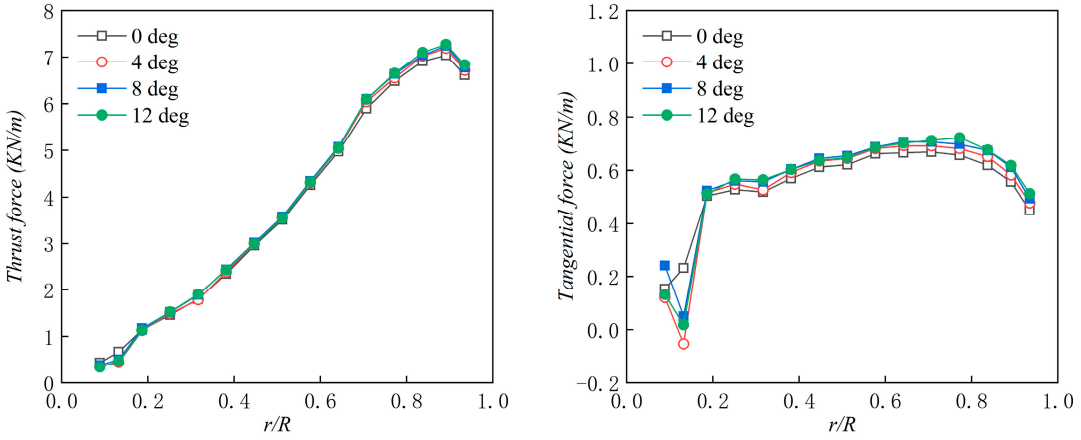


**Figure 16.** Thrust and tangential force per unit of span along the blade span for Blade 1.

Thrust force per unit of span along the rotor span for Blade 1 is shown in Figure 17. In the blade root, the thrust will fluctuate with the change of the azimuth angle, which is mainly caused by the three-dimensional flow of the blade root. In the middle of the blade, when the azimuth angle is 0-180°, the thrust is the largest at 4° tilt angle, and the thrust is the smallest at 12° tilt angle. When the azimuth angle is 180-360°, the thrust gradually decreases as the tilt angle increases. In the vicinity of the blade tip, when the azimuth angle is 0-180°, except for the tilt angle of 0°, the thrust has a change that increases first and then decreases with the change of the azimuth angle. When the azimuth angle is 180-360°, the thrust curve decreases first and then increases, and the thrust gradually decreases as the

elevation angle increases. Figure 18 shows the tangential force per unit of span along the rotor span for Blade 1. We can see that in the middle of the blade and near the tip of the blade, the tangential force of the section airfoil in the 180-360° angle range is higher than the value in the 0–180° angle range, except for the case of the 0° tilt angle. At the same time, we found that in the middle of the blade and near the tip of the blade, when the azimuth angle is 180°, the thrust and tangential force at 0° tilt are the smallest, which is mainly due to the maximum interaction between the blade and the tower at 0° tilt angle.

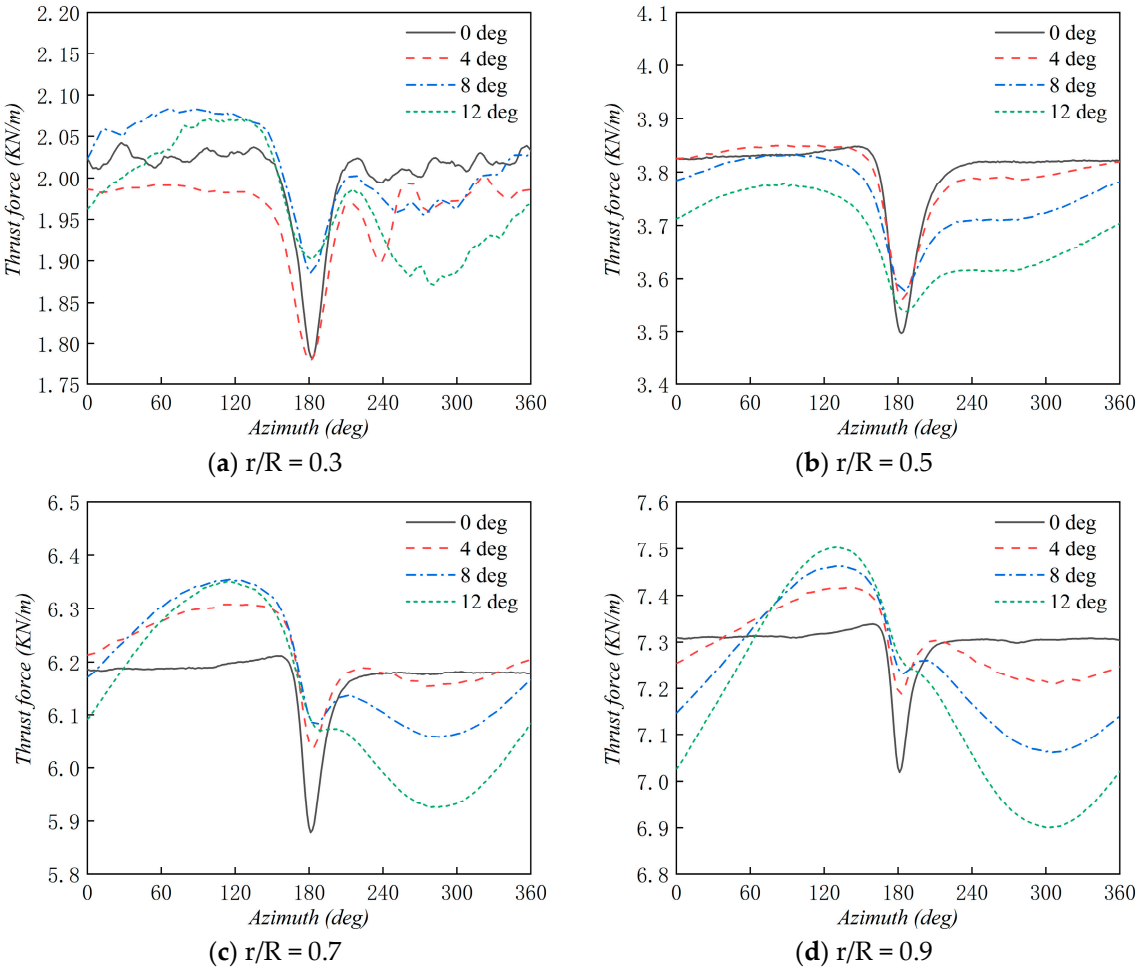


**Figure 17.** Thrust force per unit of span along the rotor span for Blade 1.

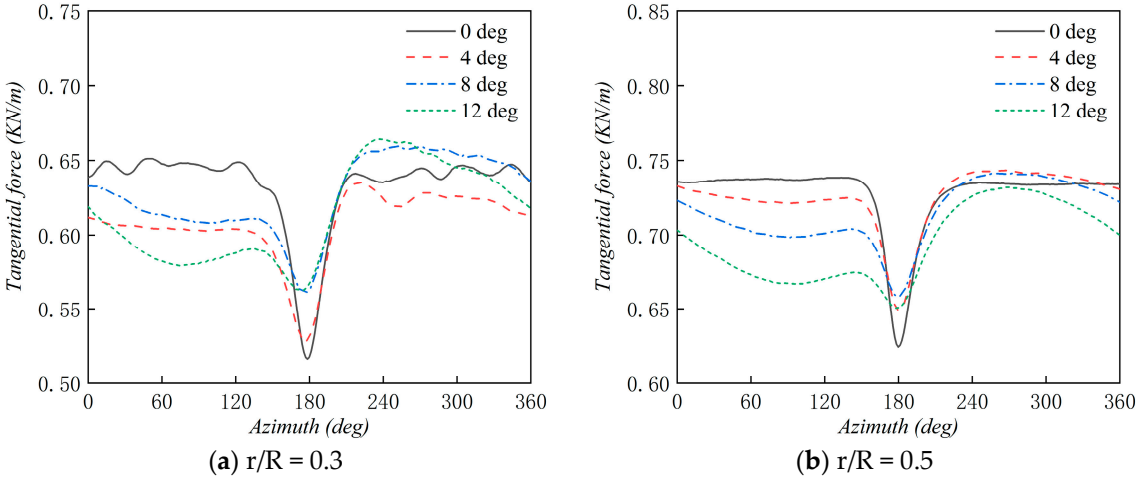


**Figure 18.** *Cont.*

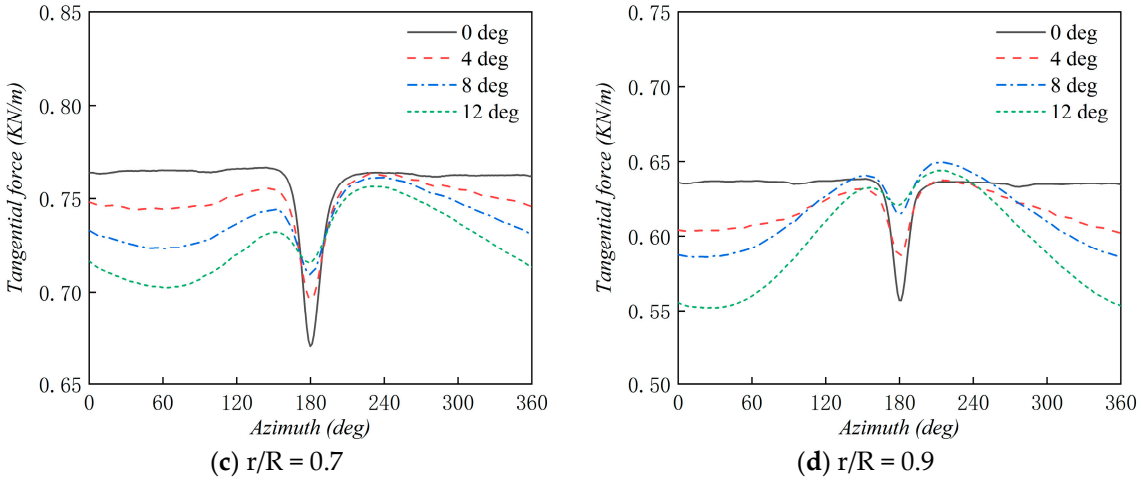


**Figure 18.** Tangential force per unit of span along the rotor span for Blade 1.

### *3.3. The Effect of the Tilt Angle on the Wind Turbine Wake*

The instantaneous isovorticities occurring when the blade is in front of the tower are presented in Figure 19. One can clearly see that these instantaneous diagrams with nacelle tilt angle shows that there is a strong flow interaction between the wake generated by the blade root, hub and tower regions. Because of the existence of the tower, there are strong unsteady flow interactions between tower vortex and blade tip vortex during downstream propagation. This interaction caused the blade tip vortex to break behind the tower. In addition, an increase in tilt angle will cause the blade tip vortex tube to tilt.

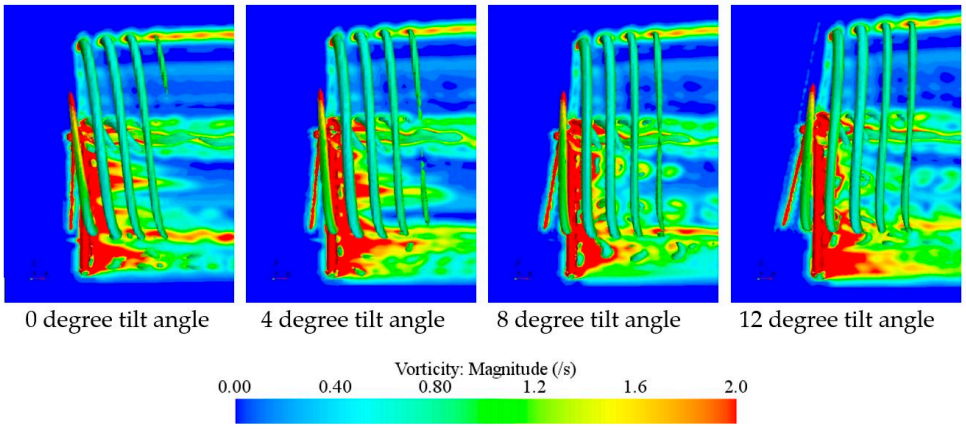


**Figure 19.** Side-view of instantaneous isovorticity contours for different nacelle tilt angles.

The instantaneous x-vorticities at different sections in four tilt angles are presented in Figure 20. We can observe that there is a clear difference in the blade tip vortex at different tilt angles. At 0 and 4° tilt angles, the blade tip vortex has only negative x-vorticities. When the tilt angle is changed to 8°, positive x-vorticity and negative x-vorticity appear in the right half of the blade tip vortex. When the tilt angle is changed to 12°, the left part of blade tip vortex is negative and right part is positive. At the same time, it can be seen that there are slight differences in the tower-generated vortexes of the four cases. By comparison, at the positions of x/D = 0.25 and x/D = 0.5, the vortex generated by the tower behind the rotor at the tilt angle of 4° is slightly less than other cases. When the tilt angle reaches 12°, the vortex generated by the tower is broken.

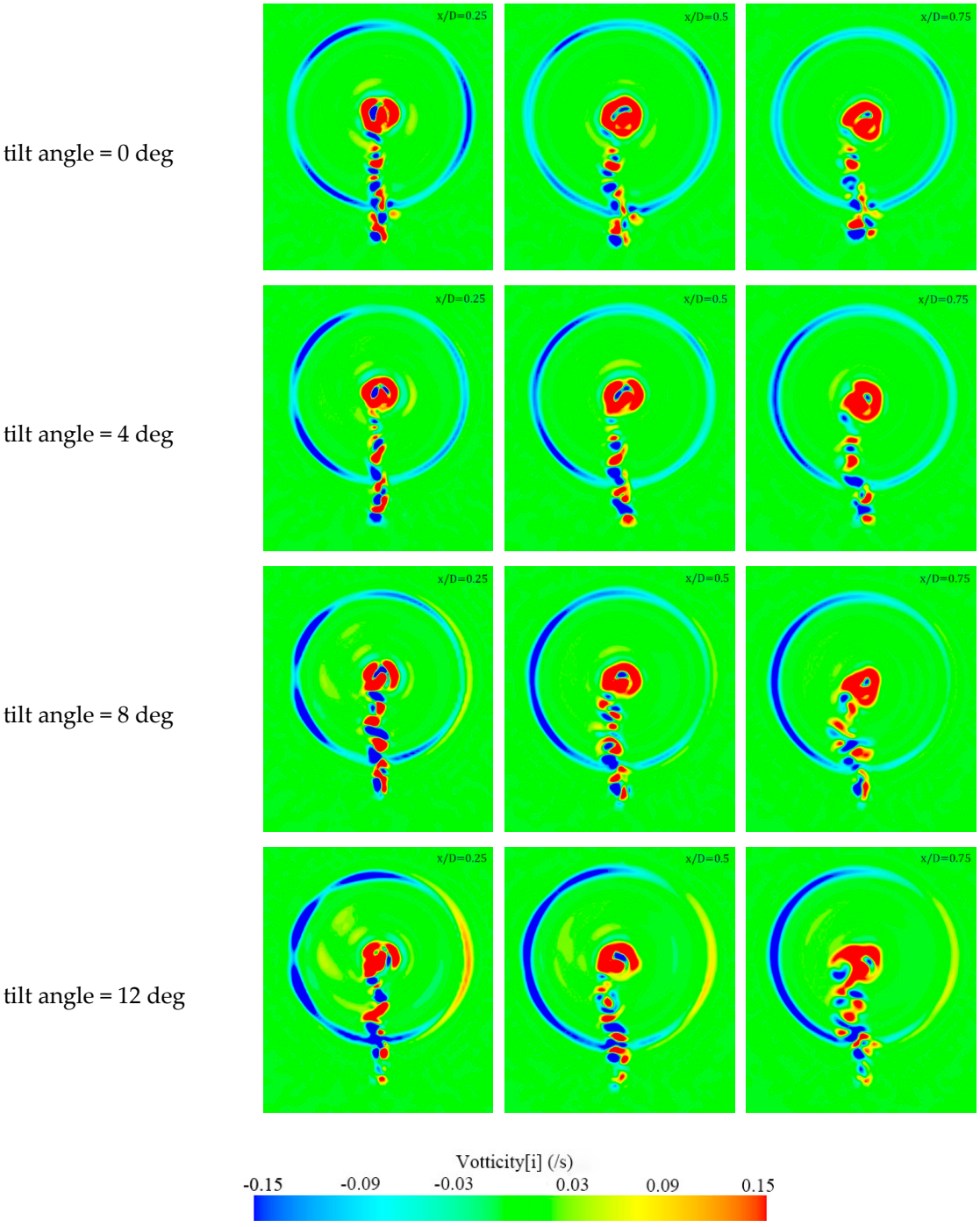


**Figure 20.** Instantaneous x-vorticities at different sections for four tilt angles.

The corresponding vertical x-velocity profiles are presented in Figure 21. When the tilt angle is 0°, as the downstream distance increases, the velocity field behind the wind turbine is approximately symmetrical about the centerline and keeps a circular shape. However, as the tilt angle increases, the velocity field behind the wind turbine shows asymmetry and gradually moves to the upper right. Meanwhile, the low-velocity region at the end of the wake gradually decreases with increasing tilt angle.

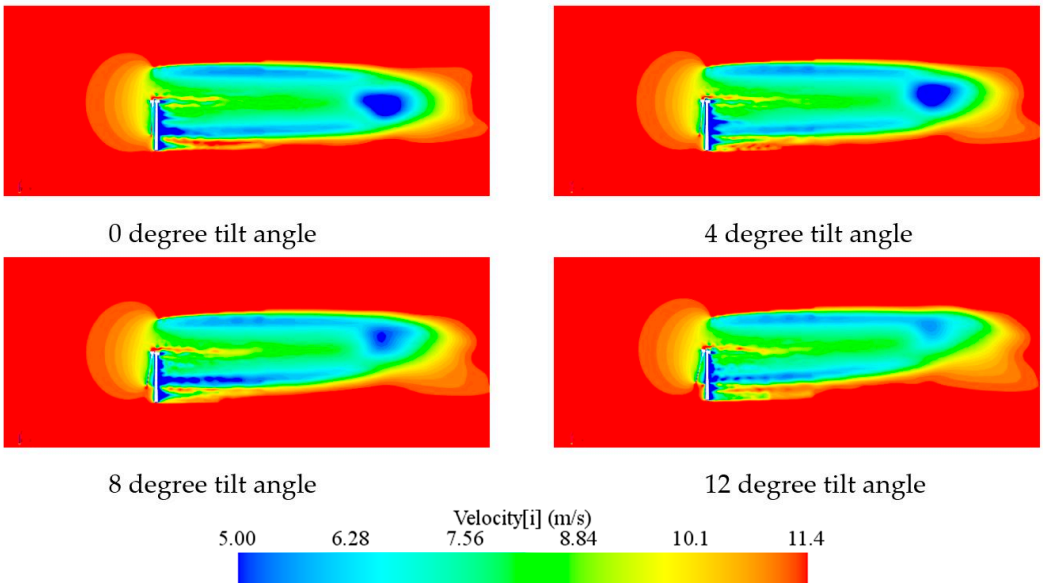


**Figure 21.** Vertical section x-velocity profiles at y = 0 m.

Figure 22 shows the distribution of instantaneous axial velocity along blade span at the wind turbine downstream positions of 0.5D, 2.5D, 3.5D and 4.5D, which represent the development of the velocity in the wake. Observing the instantaneous axial velocity distribution at the position of X/D = 0.5, it can be seen that the upper half of the curve does not change much with the tilt angle, but the lower half of the curve changes significantly with the tilt angle. In addition, it can be seen that the lower half of the curve has the smallest fluctuation at the 4° tilt angle, which means that the interaction between the blade tip vortex downstream of the wind turbine and the tower wake vortex is the weakest at a tilt angle of 4°. We can also observe a similar phenomenon in Figure 21. Observing the instantaneous axial velocity distribution at the positions of X/D = 2.5 and X/D = 3.5, we can see that as the tilt angle increases, the minimum velocity in the wake gradually increases and shifts upwards. However, at the position of X/D = 4.5, there is a slight decrease in the minimum velocity as the tilt angle increases. This is due to the upward shift of the wake-end deceleration zone.

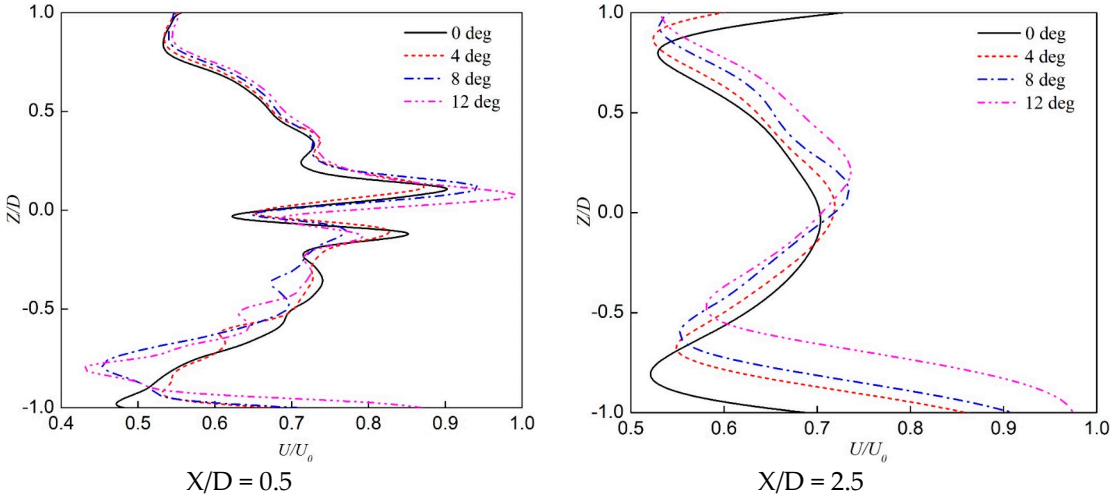


**Figure 22.** *Cont.*

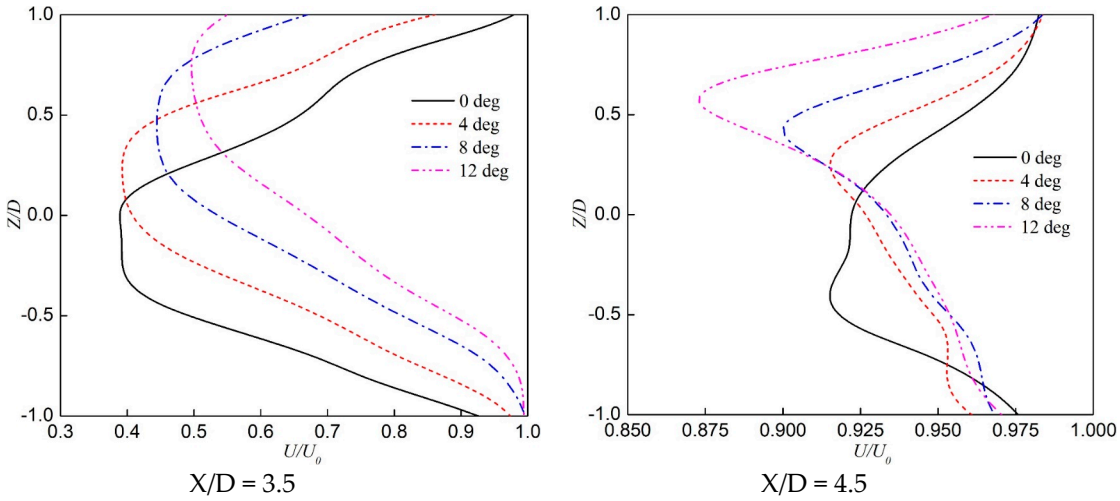


**Figure 22.** The distribution of instantaneous axial velocity along blade span at the wind turbine downstream positions of 0.5D, 2.5D, 3.5D and 4.5D.

### *3.4. Wind Shear*

The change in wind speed with height was determined according to the power function given in International Electrotechnical Commission (IEC) 61400-1 [21] and presented as follows:

$$\frac{V_Z}{V_{Z_r}} = \left(\frac{Z}{Z_r}\right)^{\gamma} \tag{12}$$

where $V_Z$ refers to the wind speed at height z, $V_{Z_r}$ refers to the reference wind speed at height $Z_r$ and $\gamma$ refers to the wind shear exponent. $Z_r$ refers to the hub height. In this study, the reference wind speed is 11.4 m/s. In this paper, wind shear exponents are 0.09, 0.2 and 0.41. The wind shear exponent of 0.09 indicates a very unstable atmospheric state, 0.20 represents a neutral state and 0.41 represents a very stable state [4].

The turbulence intensity was calculated according to the formula in IEC 61400-1 [21] and given as follows:

$$I_T = I_{ref}(0.75V_{hub} + 5.6)/V_{hub} \tag{13}$$

where $I_T$ is the turbulence intensity, $I_{ref}$ is the expected value of the turbulence intensity and $V_{hub}$ is the reference velocity at the hub. In this paper, $I_{ref}$ values are 0.12, 0.14 and 0.16. $I_{ref}$ of 0.12 represents lower turbulence characteristics, 0.14 describes medium turbulence characteristics and 0.16 describes higher turbulence characteristics.

Table 8 shows the average power along one rotation of the wind turbine after it has stabilized. It can be seen from Table 8 that, compared with uniform wind, wind shear will cause the average power of the wind turbine to decrease by about 14%. At the same time, it can be found that the average power of the 4° tilt angle is close to that of the 0° tilt angle and is higher than the average power of the 8 and 12° tilt angles under uniform wind or wind shear conditions. The deviation ($|P_a - P_m|$) of the power relative to the average power at an azimuth angle of 180° gradually decreases as the tilt angle increases (see Figure 23, Table 8). When the tilt angle reaches 8° and continues to increase, $|P_a - P_m|$ will remain unchanged. This means that as the tilt angle increases, the interaction between the blade and the tower gradually weakens. When the tilt angle exceeds 4°, the influence of the tilt angle on the interaction between the blade and the tower can be ignored. However, when the tilt angle exceeds 4°, it will cause a significant decrease in the average power of the wind turbine. Therefore, considering the power of the wind turbine and the interaction between the blade and the tower, it is more appropriate to set the wind turbine tilt angle to about 4°.

**Table 8.** Power for uniform wind and wind shear flow conditions at $V_{hub}$ = 11.4 m/s ($\gamma$ = 0.2, $I_{ref}$ = 0.14).

| Tilt Angle (°) | Average Power Pa (MW) | | | Power Pm at 180° Azimuth Angle (MW) | | | $\|P_a - P_m\|$ (MW) | |
|---|---|---|---|---|---|---|---|---|
| | Uniform Wind | Wind Shear | Error (%) | Uniform Wind | Wind Shear | Error (%) | Uniform Wind | Wind Shear |
| 0 | 4.92 | 4.20 | 14.63 | 4.73 | 4.08 | 13.74 | 0.19 | 0.12 |
| 4 | 4.91 | 4.21 | 14.26 | 4.79 | 4.15 | 13.36 | 0.12 | 0.06 |
| 8 | 4.85 | 4.18 | 13.81 | 4.78 | 4.14 | 13.39 | 0.07 | 0.04 |
| 12 | 4.75 | 4.12 | 13.26 | 4.68 | 4.08 | 12.82 | 0.07 | 0.04 |

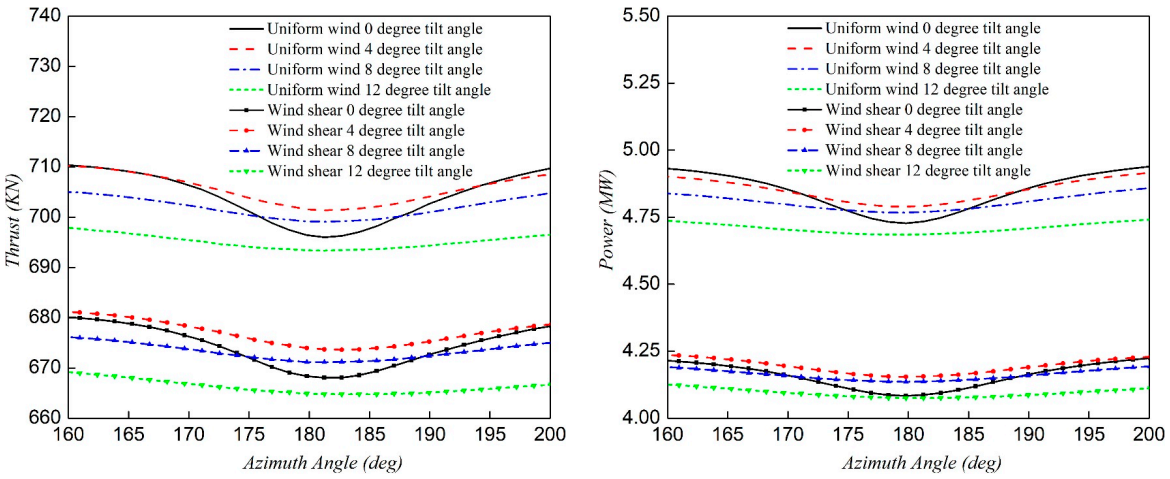


**Figure 23.** Thrust and power versus azimuth angle for various tilt angles at $V_{hub}$ = 11.4 m/s ($\gamma$ = 0.2, $I_{ref}$ = 0.14).

Figure 24 describes the influence of wind shear exponents ($\gamma$) on the aerodynamic performance of the wind turbine. It can be seen from Figure 24 that the thrust and power of the wind turbine when the wind shear exponent is 0.41 are higher than the values when the wind shear exponents are 0.09 and 0.20. It can be found from Table 9 that the average thrust and power of the wind turbine under different wind shear exponents have the smallest error when the wind shear factor is 0.41 compared with the uniform wind, and the average thrust and power of the wind turbine are almost the same when the wind shear factors are 0.09 and 0.2. In Table 9, the wind shear exponent of 0.00 means uniform wind inlet conditions. In Figure 24, it can be seen that the fluctuation of the wind turbine thrust and power curve when the wind shear factor is 0.09 is significantly higher than the other two cases. This means that the wind shear exponent has an effect on the interaction between the blade and the tower.

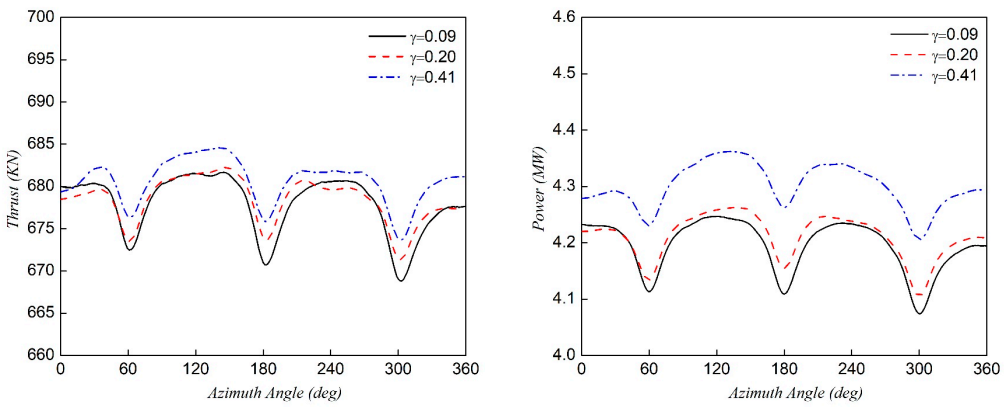


**Figure 24.** Thrust and power versus azimuth angle for various wind shear exponents ($\gamma$) at $V_{hub}$ = 11.4 m/s ($I_{ref}$ = 0.14, tilt angle = 4°).

**Table 9.** The power for various wind shear exponents ($\gamma$) at $V_{hub}$ = 11.4 m/s ($I_{ref}$ = 0.14, tilt angle = 4°).

| Wind Shear Exponents | Average Power Pa (MW) | | Average Thrust Ta (KN) | |
|---|---|---|---|---|
| | Power | Relatively Uniform Wind Error (%) | Thrust | Relatively Uniform Wind Error (%) |
| 0.00 | 4.91 | 0.00 | 709.16 | 0.00 |
| 0.09 | 4.19 | 14.66 | 677.89 | 4.41 |
| 0.20 | 4.21 | 14.26 | 678.38 | 4.34 |
| 0.41 | 4.30 | 12.42 | 680.64 | 4.02 |

At the same time, as can be seen from Figure 25, at different turbulence intensity expectations, the thrust and power of the wind turbine are basically the same. This shows that the expected value of the turbulence intensity has little effect on the thrust and power of the wind turbine. Therefore, when using wind shear to simulate a wind turbine, it is necessary to focus on the size of the wind shear exponents according to simulated working conditions.

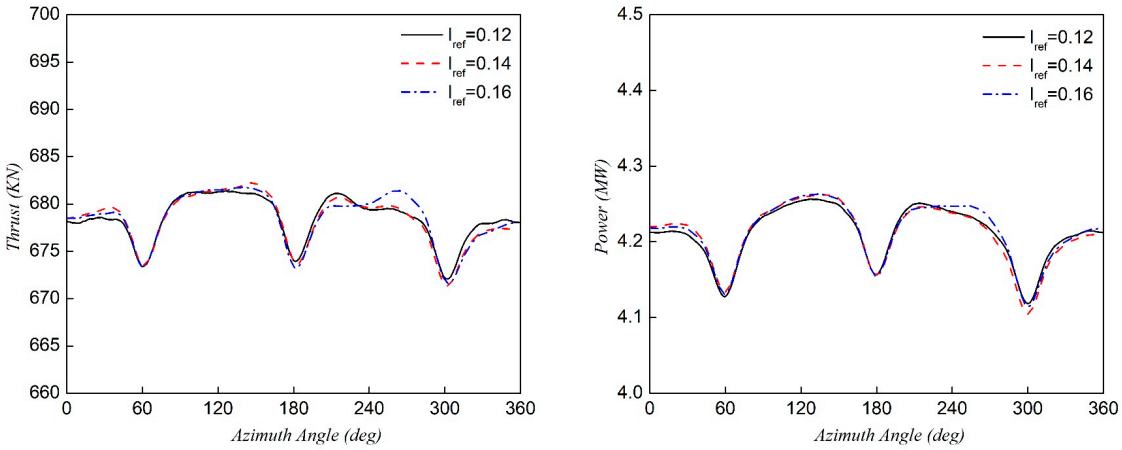


**Figure 25.** Thrust and power versus azimuth angle for various expected values of the turbulence intensity ($I_{ref}$) at $V_{hub}$ = 11.4 m/s ($\gamma$ = 0.2, tilt angle = 4°).

## 4. Conclusions

The computational fluid dynamics (CFD) method was used to simulate the aerodynamic performance of a fixed wind turbine with different tilt angles. By comparing the aerodynamic performance of a wind turbine at different tilt angles, it was found the aerodynamic performance of the wind turbine is better when the tilt angle is about 4°. The main purpose of the paper was to study the practical importance of effect of tilt angle on the aerodynamic performance of a wind turbine. The main conclusions of the paper are as follows:

1. In order to balance the power generation efficiency of the wind turbine and the interaction between the blade and the tower, the tilt angle of a wind turbine can be set at about 4° to obtain better aerodynamic performance.

2. The increase of the tilt angle will cause the load of the section airfoil to change, thus affecting the thrust and power of the wind turbine. When the blade is located in front of the tower, increasing the tilt angle will increase the load of the section airfoil. At the same time, after the tilt angle reaches 8°, the change in the load of the section airfoil with the tilt angle will not be obvious.

3. Wind shear will cause the thrust and power of the wind turbine to decrease, and the effect of the wind shear exponents on the aerodynamic performance of the wind turbine is significantly greater than the expected effect of the turbulence intensity. When performing wind turbine simulations, it is recommended to use a wind shear that is closer to that found in the real environment instead of uniform wind.

In summary, in order to ensure that a fixed wind turbine has an improved aerodynamic performance, the tilt angle of the wind turbine when installed should be about 4°. In reality, for a floating offshore wind turbine, a tilt angle of about 4° may not be appropriate, so the effect of tilt angle on a floating offshore wind turbine should be further studied in future works.

**Author Contributions:** Conceptualization, K.L.; Data curation, Q.W.; Formal analysis, Q.W.; Software, Q.W.; Supervision, Q.M.; Validation, Q.W.; Writing—original draft, Q.W.; Writing—review & editing, K.L. and Q.M. All authors have read and agreed to the published version of the manuscript.

**Funding:** This work is supported by the National Natural Science Foundation of China (Nos. 51739001, 51779049).

**Conflicts of Interest:** The authors declare no conflict of interest.

## References

1. Laks, J.H.; Pao, L.Y.; Wright, A.D. Control of wind turbines: Past, present, and future. In Proceedings of the 2009 American Control Conference, St. Louis, MO, USA, 10–12 June 2009.
2. Pao, L.Y.; Johnson, K.E. A tutorial on the dynamics and control of wind turbines and wind farms. In Proceedings of the 2009 American Control Conference, St. Louis, MO, USA, 10–12 June 2009.
3. Zhao, Q.; AlKhalifin, Y.; Li, X.; Sheng, C.; Afjeh, A. Comparative study of yaw and nacelle tilt control strategies for a two-bladed downwind wind turbine. *Fluid Mech. Res. Int. J.* **2018**, *2*, 85–97. [CrossRef]
4. Kim, H.; Lee, S.; Lee, S. Influence of blade-tower interaction in upwind-type horizontal axis wind turbines on aerodynamics. *J. Mech. Sci. Technol.* **2011**, *25*, 1351–1360. [CrossRef]
5. Guo, P. Influence analysis of wind shear and tower shadow on load and power based on blade element theory. In Proceedings of the 2011 Chinese Control and Decision Conference (CCDC), Mianyang, China, 23–25 May 2011.
6. Wang, Q.; Zhou, H.; Wan, D. Numerical simulation of wind turbine blade-tower interaction. *J. Mar. Sci. Appl.* **2012**, *11*, 321–327. [CrossRef]
7. Narayana, M. Gyroscopic Effect of Small Scale Tilt Up Horizontal Axis Wind Turbine. In *World Renewable Energy Congress VI 2000*; Elsevier: Amsterdam, The Netherlands, 2000; pp. 2312–2315. [CrossRef]
8. Zhao, Q.; Sheng, C.; Al-Khalifin, Y.; Afjeh, A. Aeromechanical analysis of two-bladed downwind turbine using a nacelle tilt control. In Proceedings of the ASME 2017 Fluid Division Summer Meeting, Waikoloa, HI, USA, 30 July–3 August 2017.
9. Abdulqadir, S.A.; Iacovides, H.; Nasser, A. The physical modelling and aerodynamics of turbulent flows around horizontal axis wind turbines. *Energy* **2017**, *119*, 767–799. [CrossRef]
10. Menter, F.R. Two-equation eddy-viscosity turbulence models for engineering applications. *AIAA J.* **1994**, *32*, 1598–1605. [CrossRef]
11. Vermeer, N.-J.; Sørensen, J.N.; Crespo, A. Wind turbine wake aerodynamics. *Prog. Aerosp. Sci.* **2003**, *39*, 467–510. [CrossRef]
12. Parente, A.; Gorle, C.; Beeck, J.v.; Benocci, C. Improved k-e model and wall function formulation for the RANS simulation of ABL flows. *Wind Eng. Ind. Aerodyn.* **2011**, *99*, 267–278. [CrossRef]
13. Tran, T.T.; Kim, D.-H. Fully coupled aero-hydrodynamic analysis of a semi-submersible FOWT using a dynamic fluid body interaction approach. *Renew. Energy* **2016**, *92*, 244–261. [CrossRef]
14. Politecnico di Milano. Qualification of innovative floating substructures for 10MW wind turbines and water depths greater than 50m. 2016. Available online: https://lifes50plus.eu/wp-content/uploads/2015/11/GA-640741_LIFES50_D3.2-mn-fix-1.pdf (accessed on 15 April 2018).
15. Miao, W.; Li, C.; Pavesi, G.; Yang, J.; Xie, X. Investigation of wake characteristics of a yawed HAWT and its impacts on the inline downstream wind turbine using unsteady CFD. *J. Wind. Eng. Ind. Aerodyn.* **2017**, *168*, 60–71. [CrossRef]
16. Jonkman, J.; Butterfield, S.; Musial, W.; Scott, G. *Definition of a 5-MW Reference Wind Turbine for Offshore System Development*; Report No. NREL/TP-500-38060; National Renewable Energy Laboratory: Golden, CO, USA, 2009.
17. Zhong, W.; Shen, W.; Wang, T.; Li, Y. A tip loss correction model for wind turbine aerodynamic performance prediction. *Renew. Energy* **2020**, *147*, 223–238. [CrossRef]

18. Yu, Z.; Zheng, X.; Ma, Q. Study on Actuator Line Modeling of Two NREL 5-MW Wind Turbine Wakes. *Appl. Sci.* **2018**, *8*, 434. [CrossRef]
19. Quallen, S.; Xing, T. An Investigation of the Blade Tower Interaction of a Floating Offshore Wind Turbine. In Proceedings of the 25th International Ocean and Polar Engineering Conference, Kona, HI, USA, 21–26 June 2015.
20. Rahimi, H.; Schepers, J.; Shen, W.; García, N.R.; Schneider, M.; Micallef, D.; Ferreira, C.S.; Jost, E.; Klein, L.; Herráez, I. Evaluation of different methods for determining the angle of attack on wind turbine blades with CFD results under axial inflow conditions. *Renew. Energy* **2018**, *125*, 866–876. [CrossRef]
21. IEC. *IEC61400-1, Wind Turbines-Part1: Design Requirements*; International Electrotechnical Commission: Geneva, Switzerland, 2005.